Journal of Applied Physics

Electrochemical characterization of GaN surface states

Cite as: J. Appl. Phys. **122**, 045302 (2017); https://doi.org/10.1063/1.4995429
Submitted: 26 February 2017 . Accepted: 10 July 2017 . Published Online: 24 July 2017

Andrea Winnerl, Jose A. Garrido, and Martin Stutzmann

ARTICLES YOU MAY BE INTERESTED IN

GaN surface states investigated by electrochemical studies
Applied Physics Letters **110**, 101602 (2017); https://doi.org/10.1063/1.4977947

Two-dimensional electron gases induced by spontaneous and piezoelectric polarization charges in N- and Ga-face AlGaN/GaN heterostructures
Journal of Applied Physics **85**, 3222 (1999); https://doi.org/10.1063/1.369664

Surface states and surface oxide in GaN layers
Journal of Applied Physics **89**, 390 (2001); https://doi.org/10.1063/1.1330553

Your Qubits. Measured.
Meet the next generation of quantum analyzers
- Readout for up to 64 qubits
- Operation at up to 8.5 GHz, mixer-calibration-free
- Signal optimization with minimal latency

Find out more

© 2017 Author(s).

JOURNAL OF APPLIED PHYSICS **122**, 045302 (2017)

Electrochemical characterization of GaN surface states

Andrea Winnerl,[1,a)] Jose A. Garrido,[2,3] and Martin Stutzmann[1]

[1]*Walter Schottky Institut and Physik Department, Technische Universität München, Am Coulombwall 4, 85748 Garching, Germany*

[2]*Catalan Institute of Nanoscience and Nanotechnology (ICN2), CSIC and The Barcelona Institute of Science and Technology, Campus UAB, Bellaterra, 08193 Barcelona, Spain*

[3]*ICREA, Pg. Llus Companys 23, 08010 Barcelona, Spain*

(Received 26 February 2017; accepted 10 July 2017; published online 24 July 2017)

In this work, we present a systematic study of the electrochemical properties of metal-organic chemical vapor deposition and hybrid vapor phase epitaxy grown n-type GaN in aqueous electrolytes. For this purpose, we perform cyclic voltammetry and impedance spectroscopy measurements over a wide range of potentials and frequencies, using a pure aqueous electrolyte and adding two different types of redox couples, as well as applying different surface treatments to the GaN electrodes. For Ga-polar GaN electrodes, the charge transfer to an electrolyte is dominated by surface states, which are not related to dislocations and are independent of the specific growth technique. These surface states can be modified by the surface treatment; they are generated by etching in HCl and are passivated by oxidation. Different surface defect states are present on N-polar GaN electrodes which do not significantly contribute to the charge transfer across the GaN/electrolyte interface. *Published by AIP Publishing*. [http://dx.doi.org/10.1063/1.4995429]

I. INTRODUCTION

In recent years, III-nitride materials—traditionally used in light-emitting diodes,[1] high power and high temperature electronic devices,[2] and short-wavelength photodetectors[3] have attracted considerable interest in photo-electrochemistry and photocatalysis due to the favorable energy position of their band edges with respect to many redox levels in liquid electrolytes.[4–9] Although its wide bandgap of 3.4 eV limits its maximum efficiency under solar illumination, GaN has been used for water splitting and CO_2 reduction. Wang *et al.* demonstrated that over-all water splitting is possible using GaN nanowires.[6] They demonstrated that the evolution of H_2 and O_2 on bare GaN nanowires is significantly faster compared to GaN powders or planar samples. By using Rh/Cr_2O_3 core-shell nanoparticles as co-catalysts, it is possible to observe steady and nearly stoichiometric evolution of H_2 and O_2 gases.[6] Furthermore, GaN has been used to directly convert CO_2 to form carbon monoxide, methane, and formic acid without the need for an extra power input except for illumination.[7,10–12] In this approach, Cu is used as the cathode and GaN is used as the anodic photoelectrode.[7] It has been successfully demonstrated that the efficiency can be increased by depositing NiO co-catalysts on the GaN photoelectrode or by using an AlGaN/GaN photoelectrode instead.[10,11] Adjusting the electrolyte composition allows to control the species and ratios of the resulting reaction products.[12] These more application oriented investigations have been accompanied by a large number of basic electrochemical studies of the GaN/electrolyte interface with the aim to learn more about the Faradaic charge exchange between GaN and different kinds of electrolytes.[13,14]

Additionally, the possibility to dope the III-nitrides n- and p-type in a controlled way enables the generation of either holes (for n-type) or electrons (for p-type) at the surface under illumination to drive oxidation or reduction reactions, respectively. Schäfer *et al.* showed that the doping type of GaN has a large influence on the chemical composition and oxygen affinity of supported Pt nanoparticles under X-ray irradiation.[8] Furthermore, Wyrzgol *et al.* demonstrated that the catalytic performance of Pt nanoparticles can be electronically controlled *via* light stimulation using n- and p-type GaN supports. Ethene hydrogenation to ethane was used as a test reaction due to its high sensitivity towards small amounts of metal and the absence of side reactions. Ethene reacts with hydrogen solely on metallic Pt, yielding a direct relation of the Pt activity to its charge density. While the conversion rate decreased for Pt on n-type GaN upon illumination, the rate was enhanced for p-type GaN. For Pt nanoparticles on p-type GaN, optical excitation results in an enhanced electron density on the nanoparticles surface. In contrast, Pt nanoparticles on illuminated n-type GaN are electron-deficient.[15]

Electronic charge transfer at semiconductor electrodes is usually strongly influenced by the presence of electronic defect states directly at or close to the semiconductor surface. The presence of such electronically active surface defects induces surface band bending, which determines the separation of photo-excited charge carriers. In addition, the defect states can be responsible for laterally inhomogeneous charging of the surface due to charge trapping. Understanding the mechanisms governing charge transfer across the GaN surface is important for a quantitative analysis of the influence of surface states on electrochemical processes and also on Schottky diodes. In previous work,[16] by combining contact potential difference (CPD) and photo-conductance measurements, we could show that these localized surface defect states play a crucial role in the kinetics of photo-generated charges. Sachsenhauser *et al.* have investigated the charge transfer

[a)]andrea.winnerl@wsi.tum.de

across the n-type SiC/electrolyte interface.[17] They performed cyclic voltammetry and impedance spectroscopy measurements over a wide range of potentials and frequencies. By using the ferricyanide/ferrocyanide redox couple, they revealed the contribution of the surface states to the charge transfer and determined the energy distribution of surface states.

In this work, we have investigated the influence of electrically active states located in the GaN bandgap on the charge transfer across the GaN/electrolyte interface. Here, we present a systematic study of metal-organic chemical vapor deposition (MOCVD) and hybrid vapor phase expitaxy (HVPE) grown n-type GaN in aqueous electrolytes using cyclic voltammetry and impedance spectroscopy measurements. To reveal the contribution of the surface states to the charge transfer and to determine their energy distribution, measurements are performed in a pure aqueous electrolyte and are compared to measurements performed in the presence of two different types of redox couples. Furthermore, the surface states are altered by applying different surface treatments, and the influence of these on the details of defect-mediated charge transfer is reported.

II. EXPERIMENTAL

Commercially available MOCVD- and HVPE-grown GaN layers were purchased from Lumilog and Kyma Technologies, respectively. The MOCVD grown (0001) n-type GaN layers exhibit a carrier concentration between $1.4 \times 10^{17}\,cm^{-3}$ and $3.0 \times 10^{18}\,cm^{-3}$ and a threading dislocation density of $5–6 \times 10^{8}\,cm^{-2}$. For the HVPE grown non-intentionally n-type doped GaN layers, the carrier concentration was between $2.1 \times 10^{16}\,cm^{-3}$ and $1.4 \times 10^{17}\,cm^{-3}$ and the dislocation density was $<5 \times 10^{6}\,cm^{-2}$. However, it should be mentioned that recent investigations have cast doubt on the lateral and in-depth homogeneity of doping levels in HVPE samples,[18] but we did not observe any noticeable effects of such inhomogeneities in the present study. Ohmic top contacts (Ti/Al/Ti/Au, 20/80/10/90 nm) were deposited by electron beam deposition and annealed in nitrogen for 5 min at 750 °C. These contacts were stable during subsequent processing of the samples (e.g., surface oxidation) and exhibited a low contact resistance which was negligible for the analysis of the electrochemical impedance measurements described below.

Surface cleaning procedures play a crucial role in most semiconductor device fabrication steps. The surface cleaning can significantly influence the metal contact resistance and stability as well as the device performance. Different *ex-situ* and *in-situ* cleaning methods have been reported and compared in the literature.[19,20] For GaN, it is known that oxygen is chemisorbed at the surface[21] and that a thin native oxide layer is formed.[22,23] Therefore, prior to metal deposition for ohmic or Schottky contacts, GaN is commonly etched in HCl or HF solutions[24–27] to reduce the native surface oxide.[19,20] For bioelectronic or biosensing applications, a stable OH-termination of the GaN surface is necessary to covalently bind molecules to the semiconductor surface; thus, wet and/or dry chemical oxidation methods are used.[5,28,29] For the present work, prior to the electrochemical measurements, different surface treatments—typically used for GaN—were performed and their influence on the electrochemical properties was investigated. As a first step, all samples were cleaned in acetone and isopropanol in an ultrasonic bath. Afterwards, the samples were either etched in HCl to remove sub-stoichiometric Ga oxide phases or oxidized by treating them for 10 min in hot H_2SO_4:H_2O_2, followed by 5 min in an oxygen plasma at 200 W. This surface oxide is not removable by etching in HCl. These samples will be referred to in the following as "etched" and "oxidized," respectively. The effect of the treatment on the chemical composition of the surface was assessed by X-ray photoelectron spectroscopy (Figs. S1 and S2, supplementary material).

Aqueous electrolytes were prepared from ultrapure water containing 50 mM TRIS (Tris(hydroxymethyl)aminomethane) and 100 mM NaCl as the supporting electrolyte. The buffer was adjusted to pH 7.3. For the measurements, either the pure TRIS electrolyte was used or 1 mM of a redox couple was added. Here, two different types of redox couples were used, namely potassium ferricyanide/ ferrocyanide (referred to as "FeCN") and ruthenium(III)/ruthenium(II) (referred to as "Ru"). Both redox couples exhibit one electron transfer and have a difference of 0.261 V in the formal redox potential.[30] Prior to the measurements, the electrolyte was degassed with a vacuum pump for 30 min, followed by thorough purging with nitrogen for 30 min to remove dissolved oxygen.

The GaN samples were mounted on a homemade PEEK holder, which exposed a circular active electrode area of $0.28\,cm^2$ and shielded the contacts as well as the electrical wiring from the electrolyte. The etched samples were measured immediately after the surface treatment, within a few minutes, to minimize native oxidation in air. The electrolyte volume was fixed to 300 ml. All measurements were performed at room temperature using a VoltaLab PGZ301 potentiostat with a three-electrode configuration in a quartz glass, with an Ag/AgCl reference electrode and a platinum wire as the counter electrode. To guarantee electrical shielding, the measurements were performed in a grounded Faraday cage. To minimize oxygen contamination, a constant flow of nitrogen was maintained over the electrolyte during the measurements. All of the cyclic voltammograms (CVs) were obtained at a scan rate of 250 mV/s. Impedance spectra were recorded at different DC biases (between –1.2 V and 0.8 V *vs.* Ag/AgCl) in single-sine mode for a frequency range between 0.1 Hz and 50 kHz, with the AC modulation amplitude set to 50 mV. The ZSimpWin software (www.princetonappliedresearch.com) was used to analyse the measured impedance data.

III. RESULTS AND DISCUSSION

The CPD is the difference between the work functions of a metal reference electrode and a semiconductor surface. In a typical CPD measurement, the CPD signal is measured as a function of time. In the dark, n-type GaN exhibits an upward band bending of approximately 1 eV due to electrons captured by the surface states.[21,31–33] Applying a bias in the dark between the GaN sample and a surface contact (electrolytic or metallic) leads to changes of charge density in the

space-charge region (SCR) and at the surface, which results in a modification of the surface band bending. Under illumination electron-hole pairs are generated, resulting in a charge redistribution within the sample. The surface photovoltage (SPV) is the corresponding photo-induced change in the CPD signal and allows the direct measurement of the change in surface band bending caused by the charge exchange between the SCR and the surface. Figure 1(a) shows a typical CPD measurement obtained for an n-type MOCVD-grown GaN sample with a doping level of $1.4 \times 10^{17}\,\mathrm{cm}^{-3}$. Under illumination, the CPD signal rises quickly to more negative values, corresponding to a SPV of about 0.65 eV, and decays slowly back to the dark value when the illumination is ceased. In previous work,[16] by combining CPD and photo-conductance measurements, we could show that in addition to surface defect states shallow defects in the SCR also play a crucial role in the kinetics of photo-generated charges. These states are responsible for the trapping of photo-generated electrons in the SCR close to the surface, which explains the slow response of the photocurrent (PC). These states are also involved in the transfer of electrons back to the surface after illumination, which results in a slow recovery of the CPD and the PC in the dark, a phenomenon known as persistent photoconductivity. These recombination processes are illustrated in Fig. 1(b), which shows a schematic view of the electronic structure near the GaN surface. To demonstrate the importance of surface states for GaN devices, Fig. 1(c) shows a comparison of the current-voltage (I-U) characteristics of Pt/GaN Schottky diodes processed on oxidized and etched GaN surfaces. For this purpose, 15 nm of Pt was deposited (by electron beam evaporation) on the MOCVD-grown GaN samples with a doping level of $1.4 \times 10^{17}\,\mathrm{cm}^{-3}$ immediately after the surface treatment. As can be seen, the surface treatment significantly affects the I-U characteristics. For the etched sample a Schottky diode behavior with an on-off ratio of about three orders of magnitude can be observed, whereas the oxidized sample shows a predominantly ohmic behavior. Thus, the observed difference in the electrical performance can be assigned to a change in the surface states due to the surface treatment, indicating that the oxidized GaN surface has a lower density of defects. The existence of a Schottky barrier in the etched sample is caused by a higher density of surface defects, inducing a stronger pinning of the Fermi level in the defect band, as indicated in Fig. 1(b). In conclusion, surface states induce a significant band bending and play a crucial role in the charge exchange between the SCR and the surface, both in the dark and under illumination, as well as in the charge transfer between GaN and a metal contact.

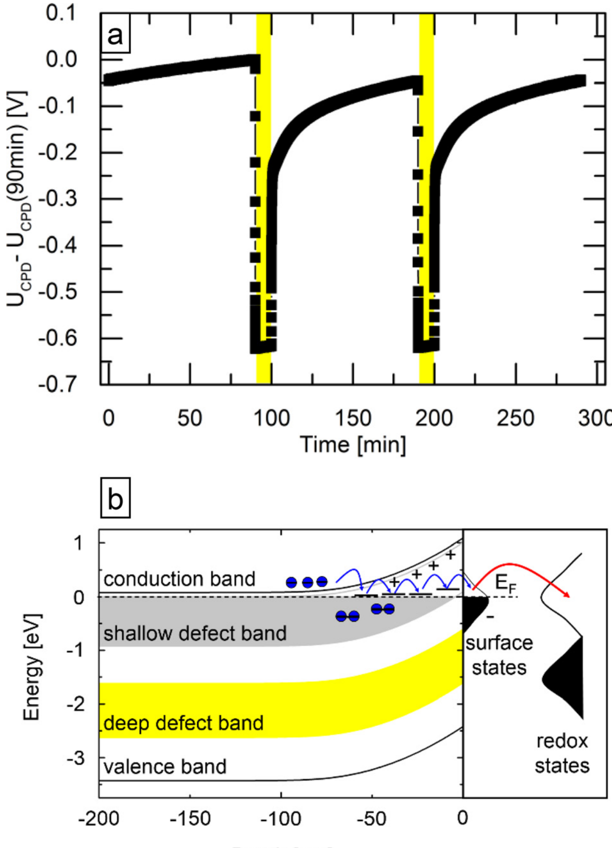

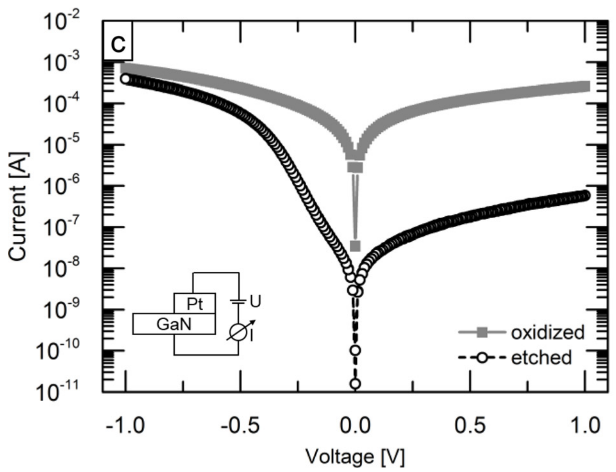

FIG. 1. (a) CPD recorded as a function of time. The illumination time intervals are highlighted in yellow. (b) Schematic view of the electronic structure near the GaN/electrolyte interface. Possible hopping processes are illustrated with blue arrows. (c) Comparison of the I-U characteristics of Schottky diodes processed on an oxidized (filled gray squares) and etched GaN surface (empty black circles).

In the following, we investigate whether or not these states are also involved in the electron transfer reactions between GaN and an aqueous electrolyte. To this end, changing the contact from metallic to electrolytic (and using MOCVD-grown GaN samples with a carrier concentration of $3.0 \times 10^{18}\,\mathrm{cm}^{-3}$), cyclic voltammograms (CVs) and impedance spectra of oxidized and etched GaN electrodes are recorded in aqueous electrolytes with and without redox couple. Figure 2(a) shows the CV curves of oxidized and etched GaN electrodes recorded in pure TRIS buffer. For both surface treatments, no Faradaic currents are observed for positive potentials. For the oxidized samples, a cathodic current arising from hydrogen evolution is observed for potentials more negative than ≈ -1.0 V *vs.* Ag/AgCl, i.e., close to the flat band potential. This behavior is expected assuming that charge transfer only involves the conduction band and the redox states in solution as depicted in Fig. 1(a). However, for the etched samples, a cathodic current is

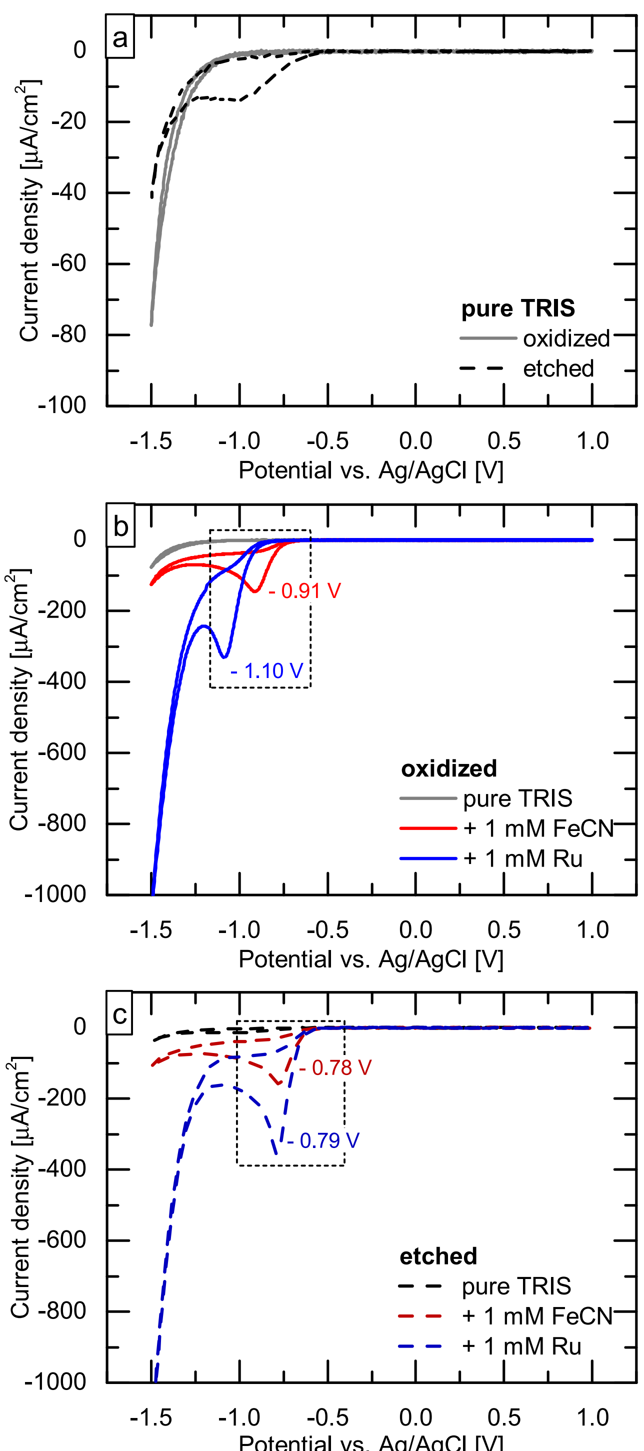

FIG. 2. (a) CVs of oxidized (solid line) and etched (dashed line) GaN electrodes, recorded at 250 mV/s in pure TRIS buffer. Comparison of CVs of (b) oxidized and (c) etched GaN electrodes, recorded at 250 mV/s in pure TRIS, in TRIS containing 1 mM FeCN, and in TRIS containing 1 mM Ru.

already observed for potentials close to –0.5 V *vs.* Ag/AgCl. In the literature, possible explanations for a non-ideal charge transfer include a potential drop across the Helmholtz layer, tunneling of electrons through the semiconductor SCR[34] or surface states with energy levels located in the band gap mediating the charge transfer across the interface.[17] Due to the rather low carrier concentration of the GaN electrodes investigated in this work, only the contribution of surface states is a reasonable explanation. Whether these states are also involved in the charge transfer across the GaN/electrolyte interface, as previously observed for SiC electrodes,[17] depends on their energetic position with respect to the redox levels in the electrolyte. In order to better reveal the contribution of the surface states, FeCN and Ru were added as redox molecules to the aqueous electrolyte. The redox molecules add unoccupied, available electronic states to the electrolyte and, therefore, change the overlap between the surface states and the redox states in the solution, which alters and possibly facilitates the charge transfer between the semiconductor and the electrolyte. Figures 2(b) and 2(c) show a comparison of CV curves of oxidized and etched GaN electrodes, respectively, recorded in different solutions with and without the redox couples. For the oxidized samples in TRIS containing a redox couple, a cathodic current is observed for less negative potentials compared to the measurement performed in pure TRIS. In the presence of FeCN, a cathodic peak is seen at –0.91 V *vs.* Ag/AgCl, and for Ru at –1.10 V *vs.* Ag/AgCl. The observed difference in the peak position is comparable to the difference in the formal redox potentials for FeCN and Ru.[30] For the etched samples, cathodic current is observed for potentials close to –0.5 V *vs.* Ag/AgCl for all three investigated buffer solutions. For both redox couples, the cathodic peak is visible at around –0.8 V *vs.* Ag/AgCl.

Considering an ideal interface, the standard theory[30,35] predicts an exponential dependence of the cathodic current on the applied potential for the charge transfer from the conduction band to a one-electron redox system. At room temperature, a slope of 59 mV/dec is expected. Figure 3 shows the semi-logarithmic plots of the CVs of oxidized [Fig. 3(a)] and etched [Fig. 3(b)] GaN electrodes in TRIS containing FeCN (red) and Ru (blue). For both surface treatments and the two different redox couples, the obtained slopes are larger than the theoretical prediction. The so-called Tafel slope corresponds to the potential variation, for which the cathodic current density is changed by one order of magnitude. In agreement with the observed peak positions in the CVs (Fig. 2), different Tafel slopes for the two redox couples are observed for the oxidized GaN electrodes, whereas the Tafel slope values are similar for the etched GaN electrodes.

Taking into account the onset of the cathodic current and the experimentally determined Tafel slopes, it can be concluded that for GaN electrodes surface states indeed mediate the charge transfer between the conduction band and the redox states in solution—for the etched GaN electrodes in all buffer solutions used, whereas for the oxidized GaN electrodes only in the presence of the redox molecules in solution. In order to determine the energy distribution of the surface states, impedance spectra are recorded for both surface treatments in all three solutions. Figure 4 shows the inverse square of the interfacial capacitance C_{int}^{-2} resulting from impedance measurements as a function of the applied bias potential U_{bias}, known as the Mott-Schottky plot. The experimental data is fitted using the equivalent circuit models presented in a previous work on SiC electrodes.[17] The experimental data is represented by symbols and the lines show fits according to the Mott-Schottky equation. For an

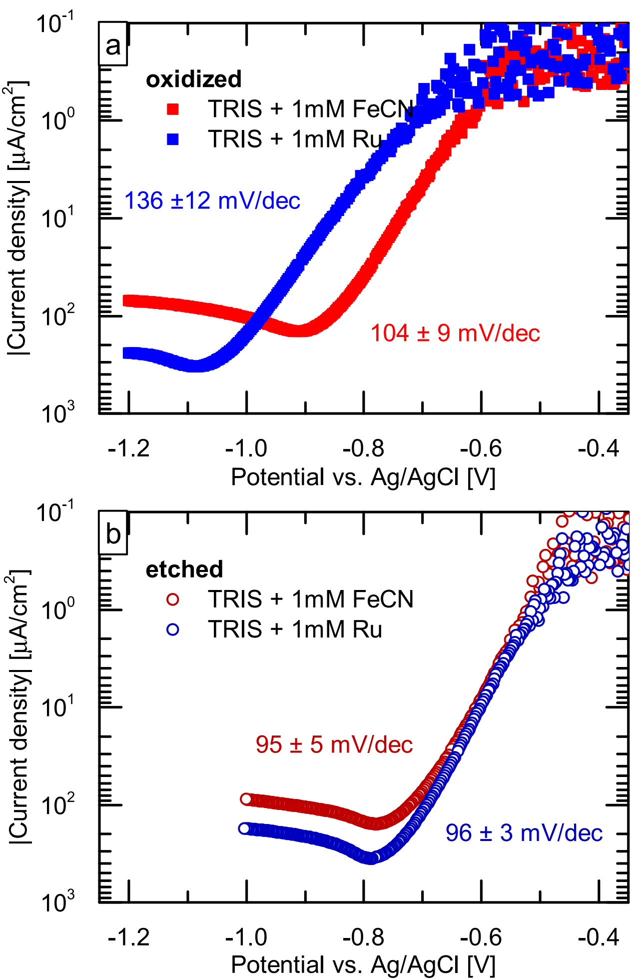

FIG. 3. Semi-logarithmic plot of CVs of (a) oxidized and (b) etched GaN electrodes, recorded at 250 mV/s in TRIS containing 1 mM FeCN (red) and 1 mM Ru (blue). The FeCN (Ru) reduction current increases exponentially with the applied bias, showing slopes of 104 ± 9 mV/dec (136 ± 12 mV/dec) and of 95 ± 5 mV/dec (96 ± 3 mV/dec) for the oxidized and etched GaN electrodes, respectively.

ideal semiconductor/electrolyte system, a linear dependence of the inverse square of the interface capacitance, C_{int}^{-2}, on the applied bias potential U_{bias} is expected.[30,35] In agreement with the CVs (Fig. 2), deviations from the predictions of the Mott-Schottky equation are observed for potentials at which significant cathodic current occurs. Figure 4(a) shows a comparison between an oxidized and an etched GaN electrode recorded in pure TRIS. As already suggested by the CV curves [Fig. 2(a)], for the oxidized sample a linear dependence is observed until –0.7 V *vs.* Ag/AgCl. For the etched sample, a significant deviation of the capacitance values from the predictions of the Mott-Schottky equation is observed for potentials more negative than –0.6 V *vs.* Ag/AgCl. The deviation from the Mott-Schottky equation is significantly larger for the etched sample than for the oxidized one. Comparing the deviations from the Mott-Schottky equation for one surface treatment in the different solutions, it can be concluded that the magnitude and potential dependence of the deviation vary with the solution used. Furthermore, the fits according to the Mott-Schottky equation can be used to determine the values of the flat band

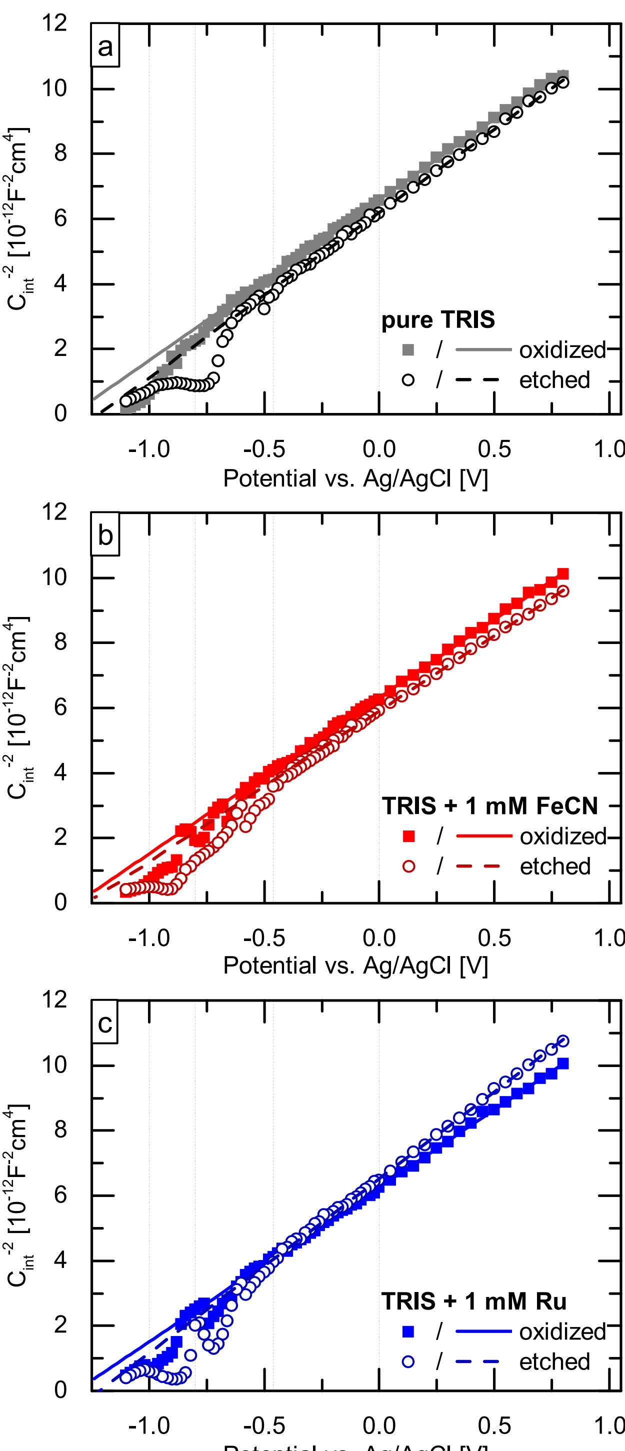

FIG. 4. Comparison of Mott-Schottky plots resulting from impedance measurements recorded in (a) pure TRIS, (b) TRIS containing 1 mM FeCN, and (c) TRIS containing 1 mM Ru for oxidized (filled symbols, solid lines) and etched (empty symbols, dashed lines) GaN electrodes. The experimental data is represented by symbols and the lines show fits according to the Mott-Schottky equation. The vertical lines represent the potential values for which representative impedance spectra are shown in Fig. 5.

potential U_{fb} and the donor density N_D. Averaging over all investigated samples for each surface treatment, a carrier concentration of $3.2 \pm 0.1 \times 10^{18}$ cm^{-3} and $3.2 \pm 0.2 \times 10^{18}$ cm^{-3} can be obtained for the oxidized and etched GaN electrodes, respectively. These values for the donor density are

in good agreement with the values obtained independently from Hall measurements. For the different surface treatments, the determined flat band potential differs by about 0.1 V; a value of -1.35 ± 0.02 V is obtained for the oxidized GaN electrodes, whereas a value of -1.26 ± 0.02 V is observed after etching the GaN electrodes. Thus, the observed onset of the cathodic current and the observed deviations from the Mott-Schottky equation start for potentials significantly more positive than the flat band potential. This further supports our previous assumption that surface states with energy levels located in the band gap are responsible for the observed non-ideal charge transfer.

As mentioned above, the impedance data is fitted using the equivalent circuit models presented in a previous work on SiC electrodes.[17] Different equivalent circuit models are necessary to describe the experimental data properly in the whole potential range, as different charge transport processes dominate the AC response depending on the applied potential. Figure 5 shows the representative impedance spectra of an oxidized and an etched GaN electrode recorded in TRIS containing 1 mM Ru for selected potential values. Contour plots of the module of the impedance and the phase in the complete potential range are provided in the supplementary material (Figs. S3 and S4). To demonstrate that the equivalent circuit models are suitable to fit the experimental data independent of the surface treatment and the buffer solution used, the analysis of the measurements in pure TRIS and TRIS containing 1 mM FeCN is provided in the supplementary material (Fig. S5). In the following, the use of different equivalent circuit models depending on the applied potential is discussed exemplarily for the oxidized sample measured in TRIS containing 1 mM Ru. For this sample [Fig. 5(a)], for potentials more positive than –0.2 V *vs.* Ag/AgCl (Region I) no charge transfer across the interface is observed and the electrode can be regarded as ideally polarized. The experimental data can be described by a serial connection of an external resistance R_S and the interface capacitance C_{int}, which in this polarization region corresponds to the space-charge capacitance. For decreasing potential (Region II, between –0.2 V and around –0.76 V *vs.* Ag/AgCl), the absolute impedance and the phase start to decrease for low frequencies. This can be assigned to the charge transfer kinetics of the redox couple reduction which starts to dominate. A parallel resistance $R_{CT,1}$ is introduced to account for the reduction process. Additionally, the capacitance is replaced by a constant phase element (CPE), as it is expected that the capacitive contribution of the surface states results in a frequency dependence of the total interface capacitance.[36,37] In Region III, for potentials more negative than –0.76 V *vs.* Ag/AgCl, the diffusion of the electroactive species in solution is rate-limiting. To account for the diffusion process, a serial connection of an additional external resistance $R_{CT,2}$ and a Warburg element W is added to the equivalent circuit. A sketch of the equivalent circuit model used to fit the data in Region III is depicted in Fig. 5(c).

The assignment of the different potential regions to the different dominant transport processes is supported by the potential dependence of the total parallel resistance R_{par}, which is depicted in Fig. 6 for oxidized [(a) and (b)] and etched [(c) and (d)] GaN electrodes in the different solutions used. The data of the oxidized sample measured in TRIS containing 1 mM Ru is shown in Fig. 6(a) in blue. The total parallel resistance summarizes the contributions of all equivalent circuit elements involved in the charge transfer across the interface. In Region II, the reduction kinetics of the redox couple at the electrode surface dominates and R_{par} decreases exponentially with bias potential with a slope of 132 ± 11 mV/dec. The values for the slope are in good agreement with the CV measurements (Fig. 3) for all the investigated samples.

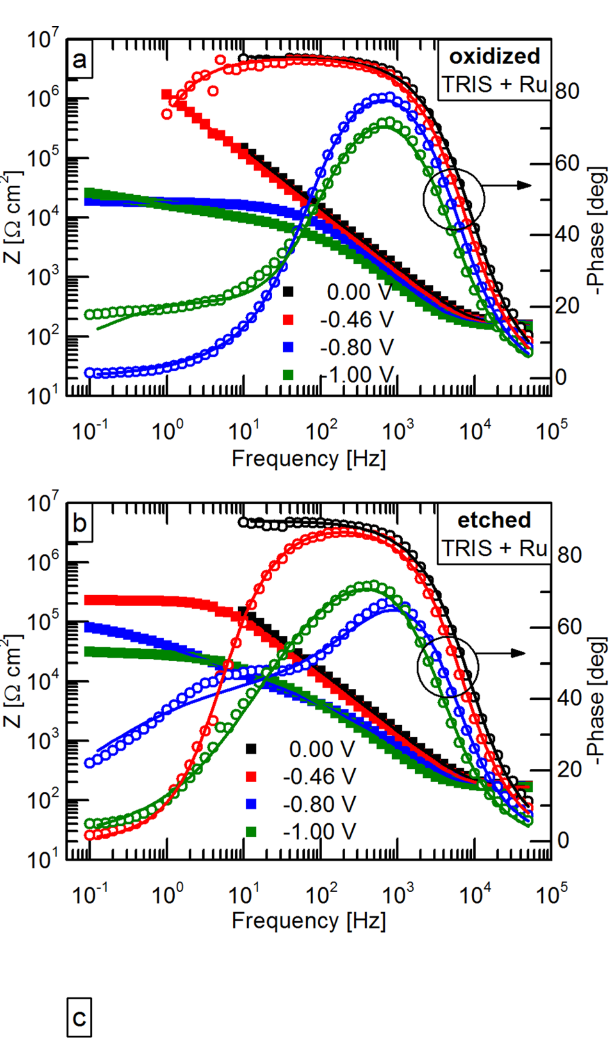

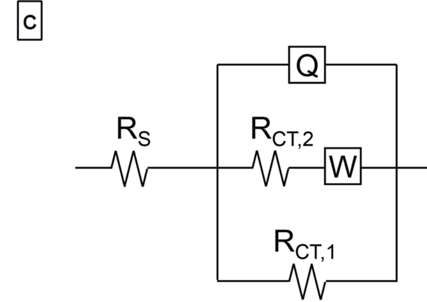

FIG. 5. Representative impedance spectra of (a) oxidized and (b) etched GaN electrodes recorded in TRIS containing 1 mM Ru. The experimental data is represented by symbols and the lines show fits according to the equivalent circuit models. Depending on the applied potential, different equivalent circuit models were used to describe the experimental data properly. The blue and green curves for the most negative potentials are obtained using the equivalent circuit model presented in (c). In the presented equivalent circuit model, Q corresponds to a capacitance (C) or a constant phase element (CPE) depending on the bias.

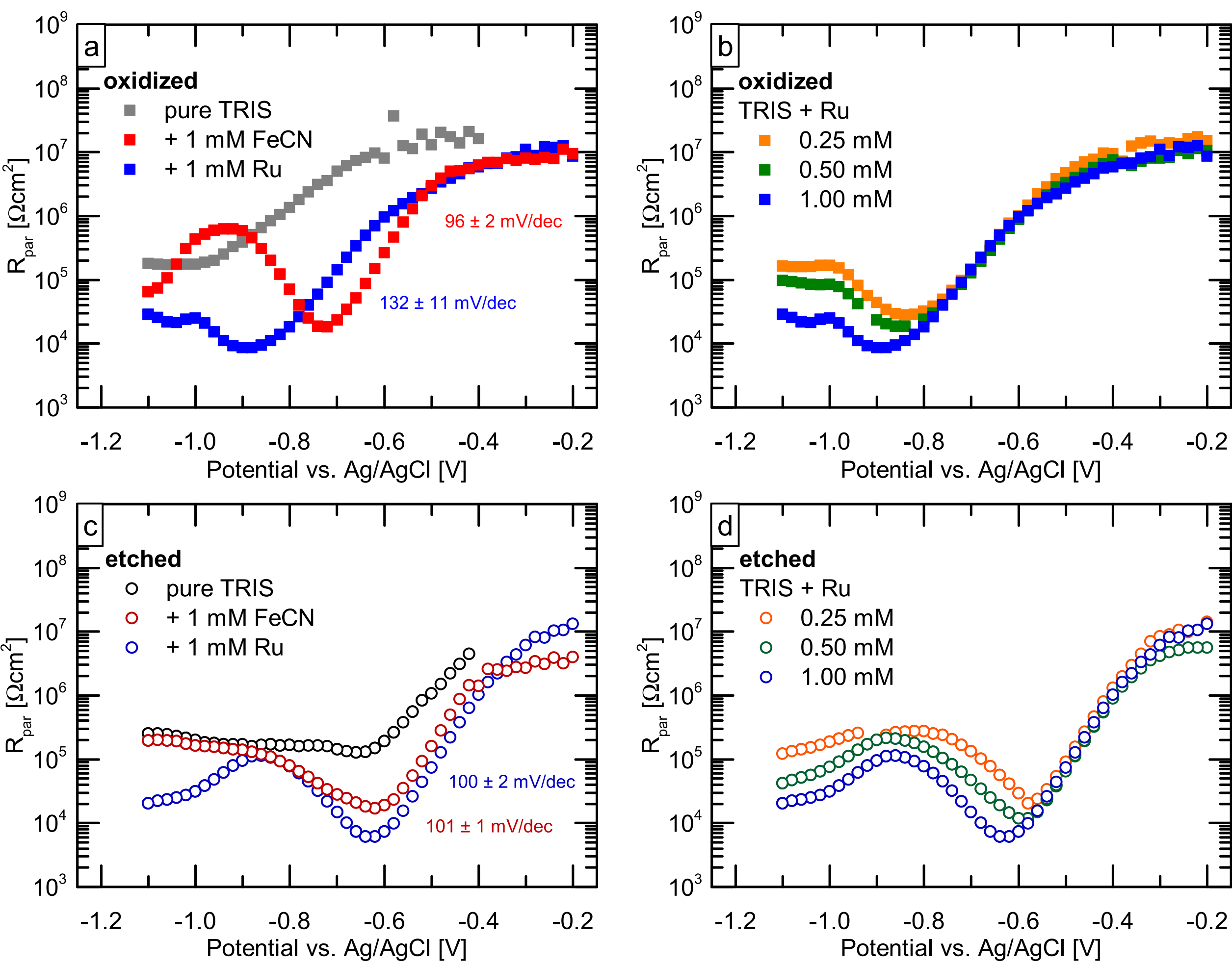

FIG. 6. Comparison of the total parallel resistance R_{par} of oxidized [(a) and (b)] and etched [(c) and (d)] GaN electrodes obtained from fitting the impedance spectra. (a) and (c) show the data obtained from measurements in pure TRIS, TRIS containing 1 mM FeCN, and TRIS containing 1 mM Ru. The data obtained from measurements in TRIS containing different Ru concentrations is depicted in (b) and (d).

In Region III, the diffusion of the redox species is rate-limiting and the total parallel resistance is frequency-dependent due to the Warburg element used in the model.[38] The total parallel resistance is calculated for a frequency of 0.1 Hz. The observed increase of R_{par} with decreasing potential can be explained by the dependence of the Warburg coefficient on the ratio of the oxidized (c_{ox}) and reduced (c_{red}) concentrations in solution. When electrons are transferred from GaN to the redox couple in solution and reduce the redox molecules, the concentration of the oxidized species drops, resulting in a large c_{red}/c_{ox} ratio and, therefore, an increase in the Warburg impedance. With decreasing applied potential, this effect becomes more and more pronounced and R_{par} continuously increases. Furthermore, measurements for different Ru concentrations were performed and the determined total parallel resistance is shown in Figs. 6(b) and 6(d) for the oxidized and etched samples, respectively. In Region II, R_{par} does not depend on the Ru concentration, whereas in Region III, R_{par} decreases with increasing Ru concentration, in agreement with our interpretation of the dominant transport mechanism: R_{par} is expected to depend on the redox couple concentration only when the diffusion of the redox species is rate-limiting.

In order to determine the energy distribution of the surface states, the potential dependence of the interface capacitance C_{int} can be used, as demonstrated by Sachsenhauser *et al.*[17] A CPE with an impedance $Z_{CPE} = \frac{1}{Q(j\omega)^{\alpha}}$ is used to account for the pseudo-capacitive contribution of the surface states. The CPE exponent α (Fig. S6, supplementary material) is close to 1 in Region I, i.e., in the potential range where the semiconductor electrode/electrolyte interface can be seen as ideal, and the interface capacitance C_{int} is given by the capacitance of the GaN SCR. In this potential range, α is independent of the applied potential. For more negative potentials, where significant deviations from the prediction of the Mott-Schottky equation are observed, α decreases. In any case, α is always larger than 0.9; therefore, according to Goossens and Schoonman the CPE parameter Q can be safely used as an approximate value for the interface capacitance C_{int}.[36] However, in the literature different models are controversially discussed for the conversion of Q into a capacitance including the values of the exponent α for the calculation. Hsu and Mansfeld suggested that the capacitance C should be equal to $Q \times (\omega_0)^{\alpha-1}$, where ω_0 is the frequency at which the imaginary part of the impedance has a maximum.[39] Figure 7 shows the resulting potential dependence of C_{int} for an oxidized and an etched GaN sample measured in TRIS containing 1 mM Ru. For comparison, the values obtained for assuming that Q is an

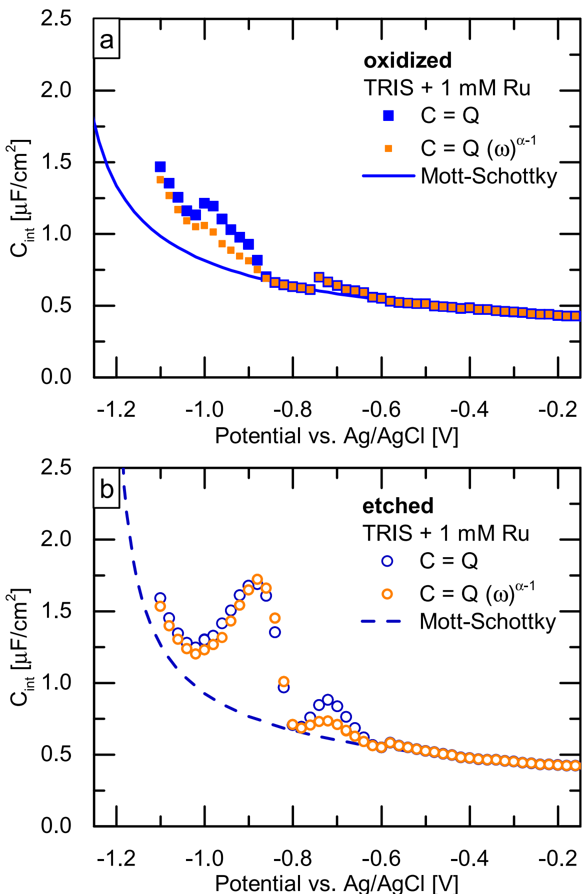

FIG. 7. Interface capacitance C_{int} of (a) an oxidized (filled squares) and (b) an etched (empty circles) GaN electrode obtained from impedance measurements recorded in TRIS containing 1 mM Ru. The symbols represent the values obtained from fitting the impedance spectra and the lines show fitting curves according to the Mott-Schottky equation. The values obtained for assuming that Q is an approximate value for the interface capacitance C_{int}[36] are shown in blue and the orange symbols represent the values obtained using the equation suggested by Hsu and Mansfeld[39] for the conversion of the CPE parameter Q into a capacitance including the CPE exponent α in the calculation.

approximate value for the interface capacitance C_{int}[36] are shown in blue and the orange symbols represent the values obtained using the equation suggested by Hsu and Mansfeld.[39] Qualitatively the same behavior and only slight differences in the absolute values of the interface capacitance C_{int} can be observed for both calculation methods. Therefore, the CPE parameter Q is used as an approximate value for the interface capacitance C_{int} in the following.

The corresponding interface capacitance C_{int} as a function of the potential for the measurements performed in pure TRIS and TRIS containing 1 mM FeCN can be found in the supplementary material (Fig. S7). For potentials more negative than –0.7 V *vs.* Ag/AgCl (–0.6 V *vs.* Ag/AgCl) for the oxidized (etched) sample, Fig. 7 shows a significant deviation of the C_{int} values from the expected dependence. This deviation can be attributed to the presence of electronic states in the band gap of the GaN electrode. When the GaN Fermi level is aligned to the electronic levels of the surface states, charge transfer can take place and, thus, an effective surface state capacitance C^*_{SS} has to be considered in parallel with the capacitance of the semiconductor SCR C_{SC}. Therefore, the effective surface state capacitance C^*_{SS}, which describes the contribution of the surface states, can be determined as the difference between the experimentally determined interface capacitance C_{int} and the theoretically predicted space-charge capacitance C_{SC}. Figure 8 shows the effective surface state capacitance derived for the oxidized [(a), (c), and (e)] and etched [(b), (d), and (f)] GaN electrodes in pure TRIS as well as TRIS containing FeCN and Ru. For the measurements performed in pure TRIS, only the etched sample shows noticeable C^*_{SS} values, with a peak centered at around –0.8 V *vs.* Ag/AgCl, in good agreement with the CVs [Fig. 2(a)]. For the etched electrodes, a second peak at more negative potentials appears in the presence of the redox couples. The position of this second peak in C^*_{SS} only slightly differs for FeCN and Ru, which is in agreement with the CVs. For the oxidized electrodes, a peak in C^*_{SS} is observed only if the buffer solution contains a redox couple. The peak positions are different for the two different redox couples and the difference is comparable to the difference in redox potential observed for the CVs (Fig. 2).[30] Comparing the different surface treatments, the etched electrodes exhibit always a higher effective surface state capacitance than the oxidized electrodes. Since a higher C^*_{SS} value corresponds to a larger number of surface states, we can conclude that etching the sample generates surface states, whereas oxidation passivates surface states to a large extent.

These observations may be understood in the following way. Below the flat band potential, charge transfer can take place *via* surface states, when the GaN Fermi level is aligned to the electronic levels of the surface states. In the case of the etched electrodes, charge transfer already takes place without the addition of redox molecules to the electrolyte, thus, there is a significant overlap between the surface states and the redox species present in the pure aqueous electrolyte and one peak can be observed in C^*_{SS} [see Fig. 8(b)]. Adding redox molecules increases the number of unoccupied, available electronic states in the electrolyte. This changes the overlap between the surface states and the redox states in solution and, therefore, the charge transfer between the semiconductor and the electrolyte is altered. Thus, two peaks are observed [see Figs. 8(d) and 8(f)] as charge transfer from the semiconductor can take place to the redox species in pure water as well as to the added redox molecules. In the case of the oxidized electrodes, the overlap between the surface states and the redox species in the pure aqueous electrolyte is not sufficiently large, therefore only one peak is observed if the buffer contains redox molecules [see Figs. 8(a), 8(c) and 8(e)]. Furthermore, the observed peak position (position of the only peak for oxidized electrodes and position of the low potential peak for etched electrodes) depends on the type of redox molecule added to the electrolyte. The energetic positions of the redox levels in the electrolyte are different for different types of redox molecules and, thus, the overlap between the surface states and the redox species depends on the type of redox molecule, which determines the position, where the peak appears in C^*_{SS}. For the oxidized electrodes, the difference in the peak position is similar to the difference in the formal redox potential, as expected. In contrast, for the etched electrodes the peak position for the two types of redox molecules only differ slightly. This might be caused by the

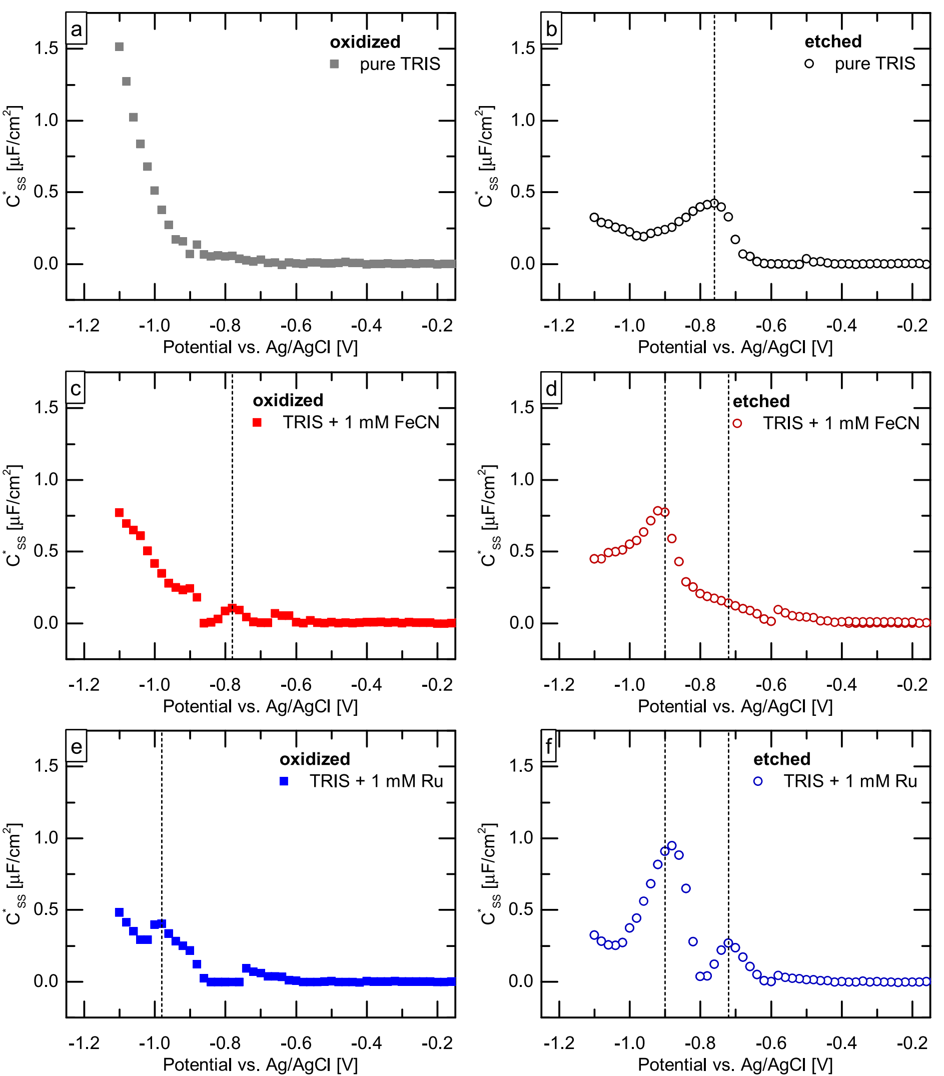

FIG. 8. Effective surface state capacitance C^*_{SS} for oxidized [(a), (c), and (e)] and etched [(b), (d), and (f)] GaN electrodes obtained from impedance measurements performed in pure TRIS, in TRIS containing 1 mM FeCN, and in TRIS containing 1 mM Ru. The vertical lines represent the position of the peaks.

energetic distribution of the surface states, which is likely to depend on the surface treatment.

Assuming a voltage of ≈1 V, the surface state density can be estimated as the effective surface state capacitance divided by the electron charge. For the etched sample measured in TRIS containing 1 mM Ru, a value of $6 \times 10^{12} cm^{-2}$ is obtained for the surface state density, whereas the surface state density is reduced by more than a factor of two after oxidation. This is an important finding as surface state densities of $10^{13} cm^{-2}$ are known to be sufficient to cause complete Fermi level pinning.[40,41]

Furthermore, to investigate if the electrochemically active surface states are related to dislocations, we performed similar measurements using the Ga-face of (0001) HVPE-grown GaN layers, which exhibit a much lower dislocation density (two orders of magnitude lower compared to MOCVD grown GaN layers). Figure 9 compares the CV curves of oxidized and etched GaN electrodes recorded in pure TRIS buffer. The data of the previously discussed MOCVD grown GaN layers are shown in black, and the results obtained for the HVPE grown samples are depicted in red. The corresponding values of the flat band potential U_{fb} and the donor density N_D obtained from impedance measurements on these samples are summarized in Table I. Independent of the growth technique, no Faradaic currents are observed at positive potentials for both the oxidized and etched samples, and for both surface treatments a similar behavior can be observed for negative potentials. After oxidation [see Fig. 9(a)], a cathodic current arising from hydrogen evolution is observed for potentials more negative than ≈ -1.0 V *vs.* Ag/AgCl (close to U_{fb}), for both the MOCVD- and HVPE-grown samples. In contrast, for both the MOCVD- and HVPE-grown samples, a cathodic current is already measurable for potentials more negative than –0.6 V *vs.* Ag/AgCl (before reaching U_{fb}) after etching the samples in HCl [see Fig. 9(b)]. Taking into account the onset of the cathodic current and the experimentally determined values of the flat band potential, this indicates that for both, MOCVD- and HVPE-grown samples, surface states with energy levels located in the bandgap mediate the charge transfer across the GaN/electrolyte interface. The corresponding interface capacitance C_{int} obtained from impedance measurements is shown in Fig. 10. The symbols represent the experimental data and the lines show fits according to the Mott-Schottky equation. The observed deviations from the Mott-Schottky equation are significantly larger for the etched sample compared to the oxidized one, for both growth techniques. As the surface treatment has a similar effect on the MOCVD and HVPE

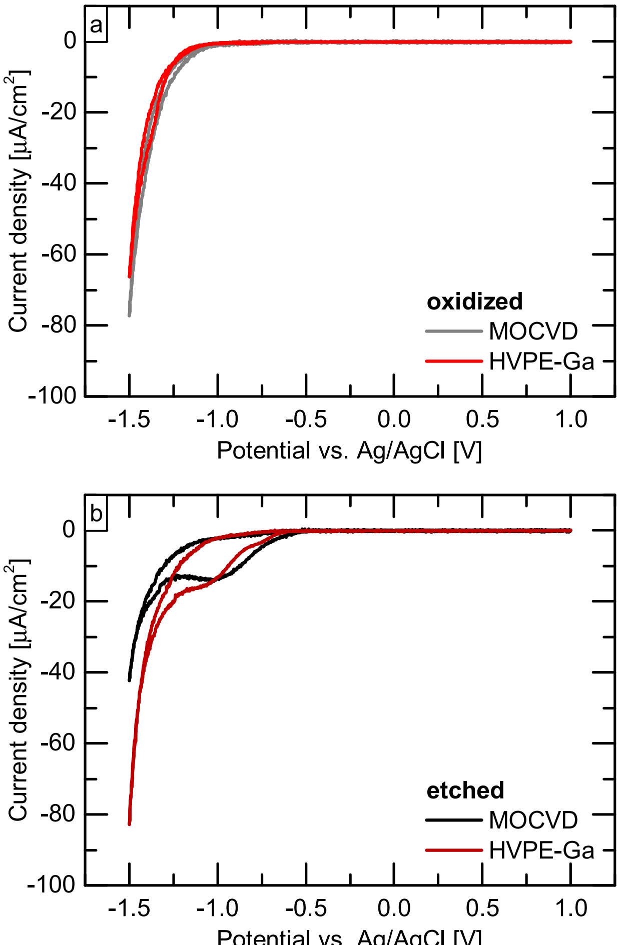

FIG. 9. Comparison of CVs of (a) oxidized and (b) etched Ga-polar GaN electrodes grown by MOCVD and HVPE recorded at 250 mV/s in pure TRIS buffer.

grown samples, it can be concluded that in both cases etching generates surface states, whereas oxidation passivates them. Moreover, it can be concluded that these electrochemically active surface states are not related to dislocations, as the effect of the surface treatment is independent of the growth techniques and, therefore, of the dislocation density.

Furthermore, measurements were also performed on the N-polar sides of the HVPE-grown GaN layers in order to investigate whether the surface states depend on the crystal polarity. Figure 11 shows a comparison of CVs of oxidized and etched GaN electrodes recorded in pure TRIS buffer. Figures 11(b) and 11(d) show a zoom to a narrower potential range of the results shown in Figs. 11(a) and 11(c),

TABLE I. Comparison of the flat band potential U_{fb} and the donor density N_D obtained from impedance measurements recorded in pure TRIS after oxidation and etching of different GaN electrodes.

	Oxidized		Etched	
Sample	U_{fb} [V]	N_D [10^{17} cm^{-3}]	U_{fb} [V]	N_D [10^{17} cm^{-3}]
MOCVD	–1.36	32	–1.24	31
HVPE Ga-polar	–1.23	0.24	–1.17	1.4
HVPE N-polar	–0.48	0.21	–0.46	7.0

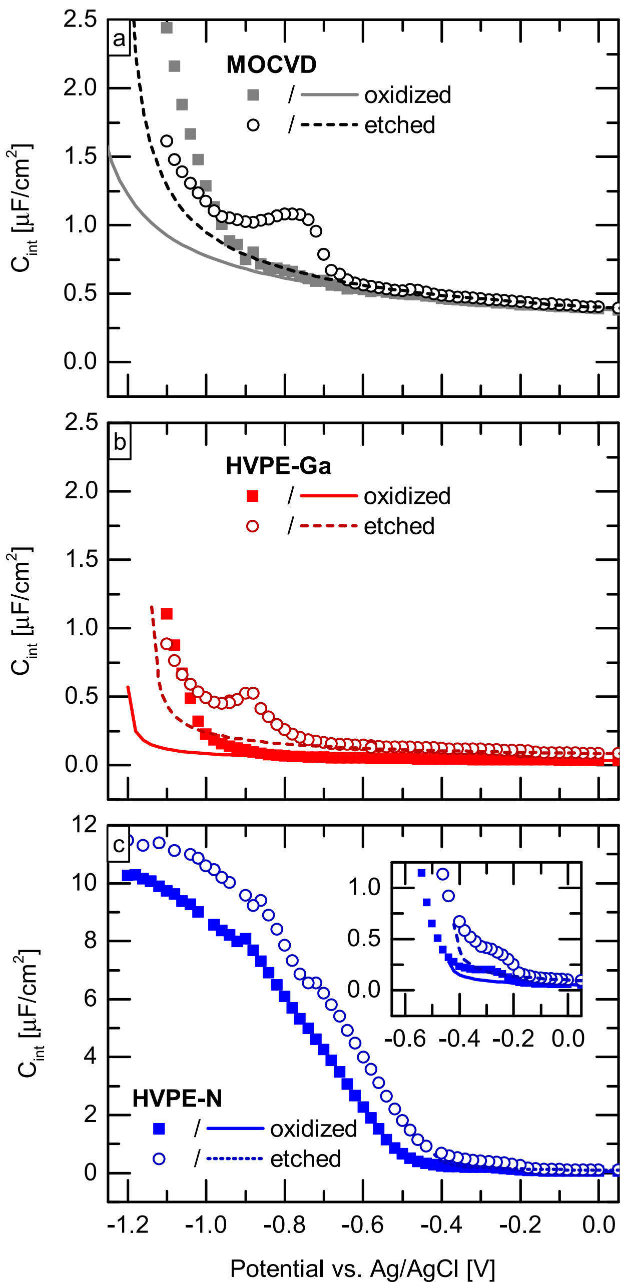

FIG. 10. Comparison of the interface capacitance of oxidized (filled symbols, solid lines) and etched (empty symbols, dashed lines) GaN electrodes obtained from impedance measurements recorded in pure TRIS buffer for (a) MOCVD, (b) HVPE-Ga, and (c) HVPE-N. The symbols represent the values obtained from fitting the impedance spectra and the lines show fitting curves according to the Mott-Schottky equation.

respectively. The results for the Ga- and N-polar sample are shown in red and blue, respectively. In order to interpret these results correctly, the corresponding values of the flat band potential have to be taken into account (see Table I). For the MOCVD grown samples and the Ga-polar side of the HVPE grown GaN electrodes, a similar value for the flat band potential of ≈ -1.2 V is determined. However, for the N-polar side of the HVPE grown GaN electrodes much smaller values of ≈ -0.5 V are obtained. Thus, the cathodic current which can be observed for potentials more negative than –0.5 V *vs.* Ag/AgCl for the oxidized and etched N-polar HVPE electrodes occurs after a flat band is reached and,

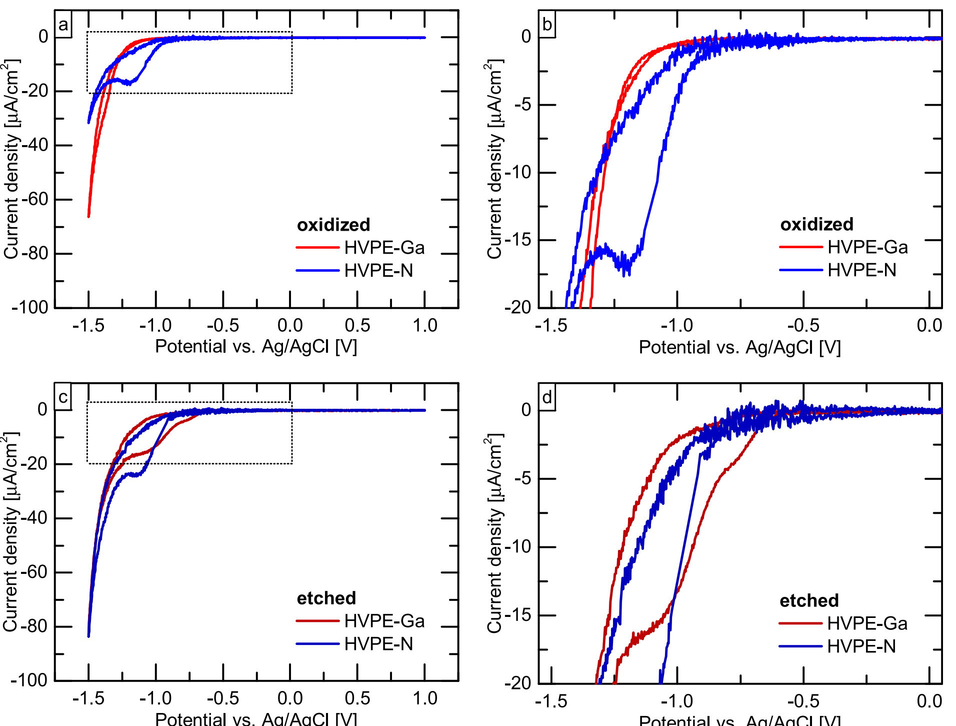

FIG. 11. Comparison of CVs of (a) oxidized and (c) etched GaN electrodes grown by HVPE recorded at 250 m/V s in pure TRIS buffer. The red lines represent the data of the Ga-polar side and the results of the N-polar side are shown in blue. (b) and (d) show a zoom to a narrower potential range.

thus, the charge transfer to the electrolyte in this potential region is not mediated by surface states [see Figs. 11(a) and 11(c)]. However, a small cathodic current larger than the typical noise level can already be measured for potentials less negative than –0.5 V *vs.* Ag/AgCl. As can be seen in Figs. 11(b) and 11(d), the cathodic current in this potential range is higher for the etched compared to the oxidized GaN electrode, similar to the effect of the surface treatment that was observed for the Ga-polar MOCVD and HVPE GaN electrodes. This indicates that also for the N-polar samples charge transfer can take place over surface states, but the resulting current is very low and, therefore, this effect can be neglected compared to the behavior observed for the Ga-polar samples. Figure 10(c) shows the resulting values of the interface capacitance obtained from impedance measurements. A very small deviation from the prediction of the Mott-Schottky equation can be observed for the oxidized and etched samples for potentials more negative than –0.2 V *vs.* Ag/AgCl in agreement with the CVs [see Figs. 11(b) and 11(d)]. In comparison to the Ga-polar MOCVD and HVPE GaN electrodes, this deviation from the theoretical prediction is much smaller. From this we can conclude, that the Fermi level pinning is weaker on the N-polar side compared to the Ga-polar side of the HVPE grown sample and the responsible defects are not electrochemically active. Thus, different surface defects are present on the Ga- and N-polar side of the HVPE grown GaN electrodes.

It is known that n-type Ga-polar GaN shows an upward band bending of approximately 1 eV due to electrons captured by surface states.[21,31–33] The origin of these electron acceptor surface states is still not well understood. As in other semiconductors, these states may be related to intrinsic defects such as dangling bonds, impurities, surface reconstruction, or random stress.[42–45] They may also originate from extrinsic sources such as atoms or molecules absorbed on the surface or defects in the surface oxide layer. Recently, Eller *et al.* investigated the influence of polarization of GaN and AlGaN on the surface band bending and the electronic surface states.[46] They suggest nitrogen vacancies or gallium dangling bonds as the surface states responsible for the observed Fermi level pinning. Our experimental data shows a similar flat band potential—corresponding to a similar surface band bending—for the etched and oxidized GaN electrodes, which is in good agreement with the value of 1 eV reported in the literature.[21,31–33] The effective surface state capacitance depends on the applied surface treatment. On the N-polar side, the Fermi level is less pinned compared to the Ga-polar side and the defects on both sides are different. On the N-polar side, the defects do not significantly contribute to the charge transfer across the GaN/electrolyte interface, whereas the defects on the Ga-polar side mediate the charge transfer to the electrolyte. These defects can be generated by etching the sample in HCl most probably by the removal of substoichiometric GaO_x, whereas oxidation passivates them to a large extent.

IV. CONCLUSION

In summary, we have investigated the influence of electrochemically active states located in the GaN bandgap on the charge transfer to an electrolyte. We performed a systematic study on MOCVD and HVPE grown n-type GaN using cyclic voltammetry and impedance spectroscopy measurements over a wide range of potentials and frequencies. To reveal the contribution of the surface states to the charge transfer and to determine their energy distribution, measurements were performed in a pure aqueous electrolyte and were compared to measurements performed in the presence of two different types of redox couples (FeCN and Ru). Two different surface treatments (etching in HCl and permanent oxidation), were applied to alter the surface states and to

investigate the influence of these on the defect-mediated charge transfer. Furthermore, the influence of the growth technique and polarity on the charge transfer between the GaN electrode and the electrolyte was investigated.

We find that the Fermi level pinning is different on the Ga- and N-polar sides of a HVPE-grown GaN electrode. The Fermi level is less pinned on the N-polar side and the responsible defects are not electrochemically active. In contrast, the surface defects on the Ga-polar side dominate the electron transfer reactions between GaN and the aqueous electrolyte, for both MOCVD and HVPE growth. These surface states can be modified by the applied surface treatment. Etching the sample in HCl generates defects, whereas they are passivated to a large extent upon oxidation. As similar results are obtained for Ga-polar MOCVD and HVPE GaN electrodes, it can be concluded, that the defects mediating the charge transfer are not related to dislocations.

SUPPLEMENTARY MATERIAL

See supplementary material for description of (i) the XPS analysis of the oxidation details of MOCVD and HVPE samples in the as-prepared, etched, and oxidized states, (ii) complete impedance data (frequency-bias maps of impedance module and phase) for the MOCVD samples in the etched and oxidized states for the three different electrolytes employed, (iii) the dependence of the constant phase element exponent on bias voltage, and (iv) the corresponding dependence of the deduced interface capacitance.

ACKNOWLEDGMENTS

Financial support from the Deutsche Forschungsgemeinschaft (DFG STU 139/12-1), TUM.solar in the frame of the Bavarian Collaborative Research Project "Solar Technologies go Hybrid" (SolTec) and the Excellence Cluster Nanosystems Initiative Munich is gratefully acknowledged.

[1]H. Morkoç and S. N. Mohammad, Science **267**, 51 (1995).
[2]M. S. Shur, Solid State Electron. **42**, 2131 (1998).
[3]G. Y. Xu, A. Salvador, W. Kim, Z. Fan, C. Lu, H. Tang, H. Morkoç, G. Smith, M. Estes, B. Goldenberg, W. Yang, and S. Krishnankutty, Appl. Phys. Lett. **71**, 2154 (1997).
[4]H. S. Jung, Y. J. Hong, Y. Li, J. Cho, Y.-J. Kim, and G.-C. Yi, ACS Nano **2**, 637 (2008).
[5]J. Howgate, S. J. Schoell, M. Hoeb, W. Steins, B. Baur, S. Hertrich, B. Nickel, I. D. Sharp, M. Stutzmann, and M. Eickhoff, Adv. Mater. **22**, 2632 (2010).
[6]D. Wang, A. Pierre, M. G. Kibria, K. Cui, X. Han, K. H. Bevan, H. Guo, S. Paradis, A.-R. Hakima, and Z. Mi, Nano Lett. **11**, 2353 (2011).
[7]S. Yotsuhashi, M. Deguchi, Y. Zenitani, R. Hinogami, H. Hashiba, Y. Yamada, and K. Ohkawa, Appl. Phys. Express **4**, 117101 (2011).
[8]S. Schäfer, S. A. Wyrzgol, R. Caterino, A. Jentys, S. J. Schoell, M. Hävecker, A. Knop-Gericke, J. A. Lercher, I. D. Sharp, and M. Stutzmann, J. Am. Chem. Soc. **134**, 12528 (2012).
[9]M. G. Kibria, H. P. T. Nguyen, K. Cui, S. Zhao, D. Liu, H. Guo, M. L. Trudeau, S. Paradis, A.-R. Hakima, and Z. Mi, ACS Nano **7**, 7886 (2013).
[10]S. Yotsuhashi, M. Deguchi, Y. Zenitani, R. Hinogami, H. Hashiba, Y. Yamada, and K. Ohkawa, Jpn. J. Appl. Phys., Part 1 **51**, 02BP07 (2012).
[11]S. Yotsuhashi, M. Deguchi, H. Hashiba, Y. Zenitani, R. Hinogami, Y. Yamada, and K. Ohkawa, Appl. Phys. Lett. **100**, 243904 (2012).
[12]M. Deguchi, S. Yotsuhashi, H. Hashiba, Y. Yamada, and K. Ohkawa, Jpn. J. Appl. Phys., Part 1 **52**, 08JF07 (2013).
[13]S. S. Kocha, M. W. Peterson, D. J. Arent, and J. A. Turner, J. Electrochem. Soc. **142**, L238 (1995).
[14]R. Dimitrova, L. Catalan, D. Alexandrov, and A. Chen, Electroanalysis **20**, 789 (2008).
[15]S. A. Wyrzgol, Ph.D. thesis, Technische Universität München, 2013.
[16]A. Winnerl, R. N. Pereira, and M. Stutzmann, Phys. Rev. B **91**, 075316 (2015).
[17]M. Sachsenhauser, I. D. Sharp, M. Stutzmann, and J. A. Garrido, J. Phys. Chem. C **120**, 6524 (2016).
[18]I. Tiginyanu, M. A. Stevens-Kalceff, A. Sarua, T. Braniste, E. Monaica, V. Popa, H. D. Andrade, J. O. Thomas, S. Raevschi, K. Schulte, and R. Adelung, ECS J. Solid State Sci. Technol. **5**, P218 (2016).
[19]L. L. Smith, S. W. King, R. J. Nemanich, and R. F. Davis, J. Electron. Mater. **25**, 805 (1996).
[20]S. W. King, J. P. Barnak, M. D. Bremser, K. M. Tracy, C. Ronning, R. F. Davis, and R. J. Nemanich, J. Appl. Phys. **84**, 5248 (1998).
[21]V. M. Bermudez, J. Appl. Phys. **80**, 1190 (1996).
[22]K. Prabhakaran, T. G. Andersson, and K. Nozawa, Appl. Phys. Lett. **69**, 3212 (1996).
[23]I. Shalish, Y. Shapira, L. Burstein, and J. Salzman, J. Appl. Phys. **89**, 390 (2001).
[24]C.-T. Lee and H.-W. Kao, Appl. Phys. Lett. **76**, 2364 (2000).
[25]A. Motayed, R. Bathe, M. C. Wood, O. S. Diouf, R. D. Vispute, and S. N. Mohammad, J. Appl. Phys. **93**, 1087 (2003).
[26]D. Qiao, L. S. Yu, S. S. Lau, J. Y. Lin, H. X. Jiang, and T. E. Haynes, J. Appl. Phys. **88**, 4196 (2000).
[27]U. Karrer, O. Ambacher, and M. Stutzmann, Appl. Phys. Lett. **77**, 2012 (2000).
[28]G. Steinhoff, M. Purrucker, O. Tanaka, M. Stutzmann, and M. Eickhoff, Adv. Funct. Mater. **13**, 841 (2003).
[29]B. Baur, G. Steinhoff, J. Hernando, O. Purrucker, M. Tanaka, B. Nickel, M. Stutzmann, and M. Eickhoff, Appl. Phys. Lett. **87**, 263901 (2005).
[30]A. J. Bard and L. R. Faulkner, *Electrochemical Methods: Fundamentals and Applications* (Wiley, New York, 2000).
[31]G. Koley and M. G. Spencer, J. Appl. Phys. **90**, 337 (2001).
[32]C. I. Wu, A. Kahn, N. Taskar, D. Dorman, and D. Gallagher, J. Appl. Phys. **83**, 4249 (1998).
[33]S. Sabuktagin, M. A. Reshchikov, D. K. Johnstone, and H. Morkoç, MRS Proc. **798** (2003).
[34]W. P. Gomes and F. Cardon, Prog. Surf. Sci. **12**, 155 (1982).
[35]R. Memming, *Semiconductor Electrochemistry* (Wiley-VCH Verlag GmbH, 2015).
[36]A. Goossens and J. Schoonman, J. Electrochem. Soc. **139**, 893 (1992).
[37]Z. Hens and W. P. Gomes, Phys. Chem. Chem. Phys. **1**, 3607 (1999).
[38]E. Barsoukov and J. R. Macdonald, *Impedance Spectroscopy: Theory, Experiment, and Applications*, 2nd ed. (Wiley, New York. 2005).
[39]C. H. Hsu and F. Mansfeld, Corrosion **57**, 747 (2001).
[40]A. J. Bard, A. B. Bocarsly, F.-R. F. Fan, E. G. Walton, and M. S. Wrighton, J. Am. Chem. Soc. **102**, 3671 (1980).
[41]H. Gerischer, J. Electroanal. Chem. **150**, 553 (1983).
[42]D. Goguenheim and M. Lannoo, Phys. Rev. B **44**, 1724 (1991).
[43]K. A. Bulashevich and S. Y. Karpov, Phys. Status Solidi C **3**, 2356 (2006).
[44]W. E. Spicer, P. W. Chye, P. R. Skeath, C. Y. Su, and I. Lindau, J. Vac. Sci. Technol. **16**, 1422 (1979).
[45]H. Hasegawa, L. He, H. Ohno, T. Sawada, T. Haga, Y. Abe, and H. Takahashi, J. Vac. Sci. Technol. B **5**, 1097 (1987).
[46]B. S. Eller, J. Yang, and R. J. Nemanich, J. Electron. Mater. **43**, 4560 (2014).